Bone Regulates Browning and Energy Metabolism Through Mature Osteoblast/Osteocyte PPARγ Expression

Julia Brun,[1] Flavien Berthou,[2] Mirko Trajkovski,[2] Pierre Maechler,[2] Michanlegelo Foti,[2] and Nicolas Bonnet[1]

Diabetes 2017;66:2541–2554 | https://doi.org/10.2337/db17-0116

Peroxisome proliferator–activated receptor γ (PPARγ) is a master regulator of energy metabolism. In bone, it is known to regulate osteoblast differentiation and osteoclast activity. Whether PPARγ expression in bone cells, particularly osteocytes, regulates energy metabolism remains unknown. Here, we show that mature osteoblast/osteocyte-specific ablation of PPARγ in mice (*Ocy-PPARγ*$^{-/-}$) alters body composition with age, namely, to produce less fat and more lean mass, and enhances insulin sensitivity and energy expenditure compared with wild-type mice. In addition, *Ocy-PPARγ*$^{-/-}$ mice exhibit more bone density, structure, and strength by uncoupling bone formation from resorption. When challenged with a high-fat diet, *Ocy-PPARγ*$^{-/-}$ mice retain glycemic control, with increased browning of the adipose tissue, decreased gluconeogenesis, and less hepatic steatosis. Moreover, these metabolic effects, particularly an increase in fatty acid oxidation, cannot be explained by decarboxylated osteocalcin changes, suggesting existence of other osteokines that are under the control of PPARγ. We further identify bone morphogenetic protein 7 as one of them. Hence, osteocytes coregulate bone and glucose homeostasis through a PPARγ regulatory pathway, and its inhibition could be clinically relevant for the prevention of glucose metabolic disorders.

Bone is a dynamic tissue that undergoes constant remodeling, balancing osteoblastic bone formation and osteoclastic bone resorption. The transcription factor, peroxisome proliferator–activated receptor (PPAR)γ, stimulates bone resorption through an increase in RANK signaling, leading to increased c-fos expression and NFATc1 signaling, which are the essential mediators of osteoclastogenesis and osteoclast activity (1). In contrast, expression and activation of PPARγ in mesenchymal stem cells promote the differentiation of these cells into adipocytes at the expense of the osteoblast lineage (2). Deletion of PPARγ in early osteoblasts, using the early mesenchymal-expressing Col 3.6 kb promoter, or osterix Cre, increases bone formation and osteoblast activity (3,4). However, the specific role of PPARγ in mature osteoblasts and osteocytes has not yet been explored. More recently, bone has been shown to regulate whole-body glucose homeostasis. Bone is known as an insulin-regulated tissue (5); but more importantly, the existence of skeletal feedback has emerged with osteocalcin, an osteoblast-derived polypeptide hormone reported to increase insulin release from β-cells and indirectly increase insulin action through enhanced release of adiponectin from adipose tissue (6–9). In addition, recent evidence also suggests a regulation of glucose metabolism by bone through osteocalcin-independent mechanisms (10,11). Browning of the adipose tissue has received considerable attention to prevent obesity and related comorbidities. Its regulation through the PPARs, and particularly, PPARγ has been put forward not only in adipose tissue (12,13) but also in liver and skeletal muscle, where it controls the production of several hepatokines (14) and myokines, respectively (15,16). The fact that bone remodeling occurs daily, in multiple locations and over extended surfaces, suggests that bone cells have a high energy demand that needs to be met. Recently, it has come to light that the skeleton is the fourth-largest glucose-consuming organ after fat, liver, and skeletal muscle (17). This glucose consumption has always been seen to be driven by osteoblast (18) and osteoclast (19) activity.

[1]Division of Bone Diseases, Department of Internal Medicine Specialties, Faculty of Medicine, Geneva University Hospital, Geneva, Switzerland
[2]Department of Cell Physiology and Metabolism, University of Geneva, and Faculty of Medicine, Centre Médical Universitaire, Geneva, Switzerland
Corresponding author: Nicolas Bonnet, nicolas.bonnet@unige.ch.

Received 30 January 2017 and accepted 29 June 2017.

This article contains Supplementary Data online at http://diabetes.diabetesjournals.org/lookup/suppl/doi:10.2337/db17-0116/-/DC1.

However, these two bone cells are under the control of osteocytes, which orchestrate bone modeling/remodeling and calcium homeostasis (20). Moreover, it is the most abundant cell in the bone tissue. Considering the role of PPARγ in the regulation of energy metabolism and bone remodeling and the high energy expenditure of the skeleton, we hypothesized that osteocytes might also be key cells for regulating energy metabolism. In the current study, we explore the mechanisms by which PPARγ expression in mature osteoblasts/osteocytes (OB-OCY) coregulates bone and glucose homeostasis. We demonstrated that osteocyte-targeted deletion of PPARγ in mice (Ocy-PPARγ$^{-/-}$) through the Dmp1-cre promoter improved glucose homeostasis by increasing browning of adipose tissue and inhibiting the development of hepatic steatosis, whereas bone frailty was partially prevented in terms of bone strength but not bone structure, independently of osteocalcin.

RESEARCH DESIGN AND METHODS

Construction of the PPARγ floxed allele (PPARγL2) has previously been described (1), and the PPARγ-deficient mice, specifically in late OB-OCY, result from a 10-Kb Dmp1-Cre recombination (*Ocy-PPARγ*$^{-/-}$), which has been crossed onto a full C57BL6J background (21). Control mice (*Ocy-PPARγ*$^{+/+}$) were constituted by a mix of PPARγLoxP$^{+/+}$ mice without DMP1-Cre and PPARγLoxP$^{-/-}$ mice with DMP1-Cre. The two genotypes of control mice did not exhibit significantly different phenotypes. Mice were maintained on a 12-h light/dark cycle at an ambient temperature of 22–25°C. In an aging and high-fat experiment to measure dynamic indices of bone formation, mice were injected with calcein intraperitoneally at 10 mg/kg at 9 and 2 days before euthanasia. The animals were killed and blood was collected for serum measurements.

Aging Experiment

From 3 to 6 months of age, *Ocy-PPARγ*$^{+/+}$ and *Ocy-PPARγ*$^{-/-}$ male mice were analyzed (n = 8 per group). Six supplemental mice per genotype were used to investigate insulin signaling in organs. Mice were injected intraperitoneally with 150 mU/g insulin (n = 3 per genotype) (NovoRapid; Novo Nordisk) or PBS (n = 3 per genotype) 40 min before sacrifice as previously validated (14).

High-Fat Experiment

From 4 to 6 months of age, *Ocy-PPARγ*$^{+/+}$ and *Ocy-PPARγ*$^{-/-}$ male mice received a high-fat diet (HFD) (60% fat; Kliba 2127 [Supplementary Table 1]) (n = 8 per group). An additional group received a chow diet (10% fat; Kliba 2125 [Supplementary Table 1]) for histological analysis (n = 6 per genotype).

In Vitro Experiment

Primary Osteoblast Cultures

Osteoblasts were isolated from long bones of *Ocy-PPARγ*$^{-/-}$ and *Ocy-PPARγ*$^{+/+}$ mice as previously described (22). Osteoblasts were seeded at 60,000 cells per well in 12-well plates. At day 21, RNA was extracted to confirm the expression of DMP1 and the existence of osteocytic markers. Conditioned medium (CM) was collected every 24 h.

Primary Adipocyte Culture

The stromal vascular fraction cells from white fat tissue and brown fat tissue were isolated as previously described (23). Primary stromal vascular fraction cells were seeded at 300,000 cells/well in 24-well plates. On confluence, the cells were induced to differentiate for 3 days with DMEM containing 10% FCS, 1 μmol/L dexamethasone, 500 μmol/L isobutylmethylxanthine, 1 μg/mL insulin, 125 μmol/L indomethacin, 1 nmol/L triiodothyronine (Gibco Life Technology), 1 μmol/L rosiglitazone (Santa Cruz Biotechnology), and CM of OB-OCY culture. Then the induction medium was replaced with DMEM containing 10% FCS, 1 μg/mL insulin, and 1 nmol/L triiodothyronine at days 3 and 5. Cells were stopped at 7 days for Oil Red O and gene expression analyses.

3t3L1 Adipocyte Cell Line Culture

3t3L1 adipocyte cell line was cultured as previously described (24). Cells were seeded at 5,000 cells/well in 24-well plates. Cells were stopped at 7 days for Oil Red O and gene expression analyses. At day 0, i.e., at confluency, we split the well into different groups: *1*) one still under DMEM, *2*) culture with *Ocy-Pparγ*$^{+/+}$ CM, *3*) *Ocy-Pparγ*$^{+/+}$ CM plus recombinant BMP7 (50 ng/mL), *4*) *Ocy-Pparγ*$^{+/+}$ CM plus recombinant BMP7 (150 ng/mL), *5*) *Ocy-Pparγ*$^{-/-}$ CM, and *6*) *Ocy-Pparγ*$^{-/-}$ CM plus BMP7-neutralizing antibody (5 μg/mL).

Primary Hepatocyte Culture

Primary hepatocytes were isolated from wild-type (WT) mouse liver as previously described (25). Primary hepatocytes were seeded at 300,000 cells per well in collagen-coated 12-well plates and cultured in Williams' Medium E supplemented with 10% FBS, 1% L-glutamine, 1% penicillin/streptomycin, 10^{-9} mol/L insulin, and 10^{-6} mol/L dexamethasone. Five hours after plating, cells were incubated for 2 days with conditioned media from Ocy-PPARγ$^{+/+}$, *Ocy-PPARγ*$^{-/-}$, and *Ocy-Pparγ*$^{-/-}$ plus BMP7-neutralizing antibody (5 μg/mL) to OB-OCY. Hepatosteatosis was induced by adding into these media a mix of 200 μmol/L oleic acid: palmitic acid (ratio 3:1).

Primary Islet

Pancreatic islets were isolated from male C57BL/6 mice by collagenase digestion as previously described (26) and cultured in RPMI-1640 medium supplemented with 5% heat-inactivated FCS, 10 mmol HEPES, 1 mmol sodium pyruvate, 50 μmol 2-mercaptoethanol, and antibiotics. Batches of 10 handpicked islets/well were cocultured for 4 days with *Ocy-PPARγ*$^{-/-}$ and *Ocy-PPARγ*$^{+/+}$ primary OB-OCY. Insulin secretion measurements were measured by radioimmunoassay (Linco Research, Inc., St. Charles, MO) using rat insulin as standard.

Investigations

For glucose, insulin, and pyruvate tolerance tests (GTT, ITT, and PTT, respectively), after 6 h starvation, mice were administered intraperitoneally with glucose (1.5 g/kg; Grosse Apotheke Dr. G. Bichsel, Interlaken, Switzerland), insulin (0.5 units/kg), or pyruvate (2 g/kg; Sigma), and glycemia was measured from tail blood before the injection and at 15, 30, 60, 90, and 120 min after the injection. Area under the curve (AUC) was calculated relative to baseline glucose for each genotype. Microcomputed tomography scans (UCT40; Scanco Medical AG, Basserdorf, Switzerland), hyperinsulinemic-euglycemic clamp, 2-[^{14}C]deoxyglucose uptake, metabolic cage (LabMaster calorimetry; TSE Systems, Homburg, Germany), positron emission tomography (PET)/computed tomography (CT) (Triumph microPET/SPECT/CT system; Trifoil, Chatsworth, CA), histomorphometry (RM2155 Rotary Microtome; Leica, Wetzlar, Germany), immunohistochemistry, real-time PCR, Western blotting, and a three-point bending test (Instron 1114; Instron Corp., High Wycombe, U.K.) were performed as previously described (14,27,28).

Data Analysis

Normal distribution of the data were verified by the Levene test. We then tested the effects of genotype in chow diet and HFD by a one-way ANOVA.

To compare the effect of genotype/diet, we used a two-way ANOVA. As appropriate, post hoc testing was performed using Fisher protected least squares difference. ANCOVA analyses were performed for the calorimetric data. Differences were considered significant at $P < 0.05$. Data are presented as mean ± SEM.

RESULTS

PPARγ Deletion in Osteocytes Induced a High–Bone Mass and Low–Fat Mass Phenotype

PPARγ expression increased with osteoblast differentiation into osteocytes in vitro and its expression was inducible by rosiglitazone (Fig. 1*A* and *B*). Immunostaining confirmed that PPARγ was also expressed in osteocytes in vivo (Fig. 1*C*). To achieve a genetic deletion of PPARγ in late osteoblasts/early osteocytes, we crossed Dmp1-Cre mice with homozygous PPARγ-floxed mice to remove the loxP-flanked PPARγ alleles only in these cells. Immunohistochemistry, Western blot, and RT-PCR confirmed tissue and cell specificity of PPARγ deletion in osteocytes (Fig. 1*C–F*). As reported in the literature, Dmp1-Cre also induced a partial deletion of PPARγ in the skeletal muscle but not in the brain or intestine. Lengths of femurs or tibiae did not differ between genotypes (data not shown). However, an examination of the body composition via DEXA for small animals (PIXImus) revealed more femoral bone mineral density (BMD) at the age of 3 months in Ocy-PPARγ$^{-/-}$ compared with WT littermates (Ocy-PPARγ$^{+/+}$), which remained significant with aging (Fig. 2*A*). With age (6 months), both trabecular and cortical bone structure respectively at distal and midshaft femur significantly increased in Ocy-PPARγ$^{-/-}$ versus Ocy-PPARγ$^{+/+}$ mice (Fig. 2*B–E*). These characteristics resulted from a higher bone formation rate (BFR) at the trabecular and periosteal surfaces in Ocy-PPARγ$^{-/-}$ mice, whereas BFR was unchanged at the endosteal surface, and circulating levels of total and decarboxylated osteocalcin were similar in Ocy-PPARγ$^{-/-}$ and Ocy-PPARγ$^{+/+}$ mice (Fig. 2*F–J*; Supplementary Table 2). Bone formation effects were mainly attributed to an increase in osteoblast activity rather than an increase in osteoblast number, as shown by an increase in mineralization apposition rate and an unaffected mineralization surface on bone surface (MS/BS), mineralization perimeter on bone perimeter (MPm/BPm), and osteoblast numbers (Supplementary Table 2). Bone resorption marker, such as carboxyterminal collagen crosslinks (CTX), was significantly decreased in Ocy-PPARγ$^{-/-}$; regardless, osteoclast surface on bone surface was not different between groups (Fig. 2*K* and *L*). For understanding of the mechanism by which PPARγ deletion in osteocytes increases BFR and decreases resorption, mRNA was extracted from the femur. Gene expression analyses in the osteocytic fraction of cells showed that Sost (sclerostin) mRNA levels were 33% lower in Ocy-PPARγ$^{-/-}$ compared with Ocy-PPARγ$^{+/+}$ (Fig. 2*M*). Apoptotic gene expression such as Caspase 3, Bcl2, and Bax were unchanged (Supplementary Table 3). In the osteoblastic fraction, both Runx2 and Opg levels were significantly higher in Ocy-PPARγ$^{-/-}$: 19.2% and 197.6%, respectively, versus Ocy-PPARγ$^{+/+}$ (Fig. 2*N* and *O*). Furthermore, primary mesenchymal stem cells from Ocy-PPARγ$^{-/-}$ differentiated in vitro into more mature osteoblasts, as shown by higher alkaline phosphatase levels in Ocy-PPARγ$^{-/-}$ after 21 days of culture when Dmp1 was expressed (Fig. 2*P*). Furthermore, gene expression of osteoblast markers such as Opg/Rankl, Runx2, osteocalcin (Bglap), Glut1, Glut 4, Fox2, PPARα/d, and Bmp7 was higher in Ocy-PPARγ$^{-/-}$ compared with Ocy-PPARγ$^{+/+}$, whereas E11, an early osteocyte marker, was lower (Fig. 2*Q*). These data indicated that osteocyte expression of PPARγ regulates both osteoblast differentiation/function and osteoclast resorption.

PPARγ Deletion in Late OB-OCY Increased Energy Metabolism

At 3 months of age, lean and fat mass percentages as well as glucose levels measured in response to GTT were unaffected by PPARγ deletion (Fig. 3*A–C*; Supplementary Fig. 1). However, with age (6 months), Ocy-PPARγ$^{-/-}$ gained less fat mass and more lean mass than Ocy-PPARγ$^{+/+}$ with a similar body weight gain, respectively, of 12.0% and 12.5% (Fig. 3*A–C*). At sacrifice, organ weights indicated a lower liver and epididymal white adipose tissue (eWAT) in Ocy-PPARγ$^{-/-}$ compared to Ocy-PPARγ$^{+/+}$ (Supplementary Fig. 2). Glycemic control was better in Ocy-PPARγ$^{-/-}$ mice compared with Ocy-PPARγ$^{+/+}$, with enhanced glucose tolerance (analyzed by GTT) and insulin sensitivity (measured by ITT) (Fig. 3*D–F*). Metabolic cage profiling showed more VO_2 consumption, a higher respiratory exchange ratio (RER), and more heat production in Ocy-PPARγ$^{-/-}$ mice compared to Ocy-PPARγ$^{+/+}$,

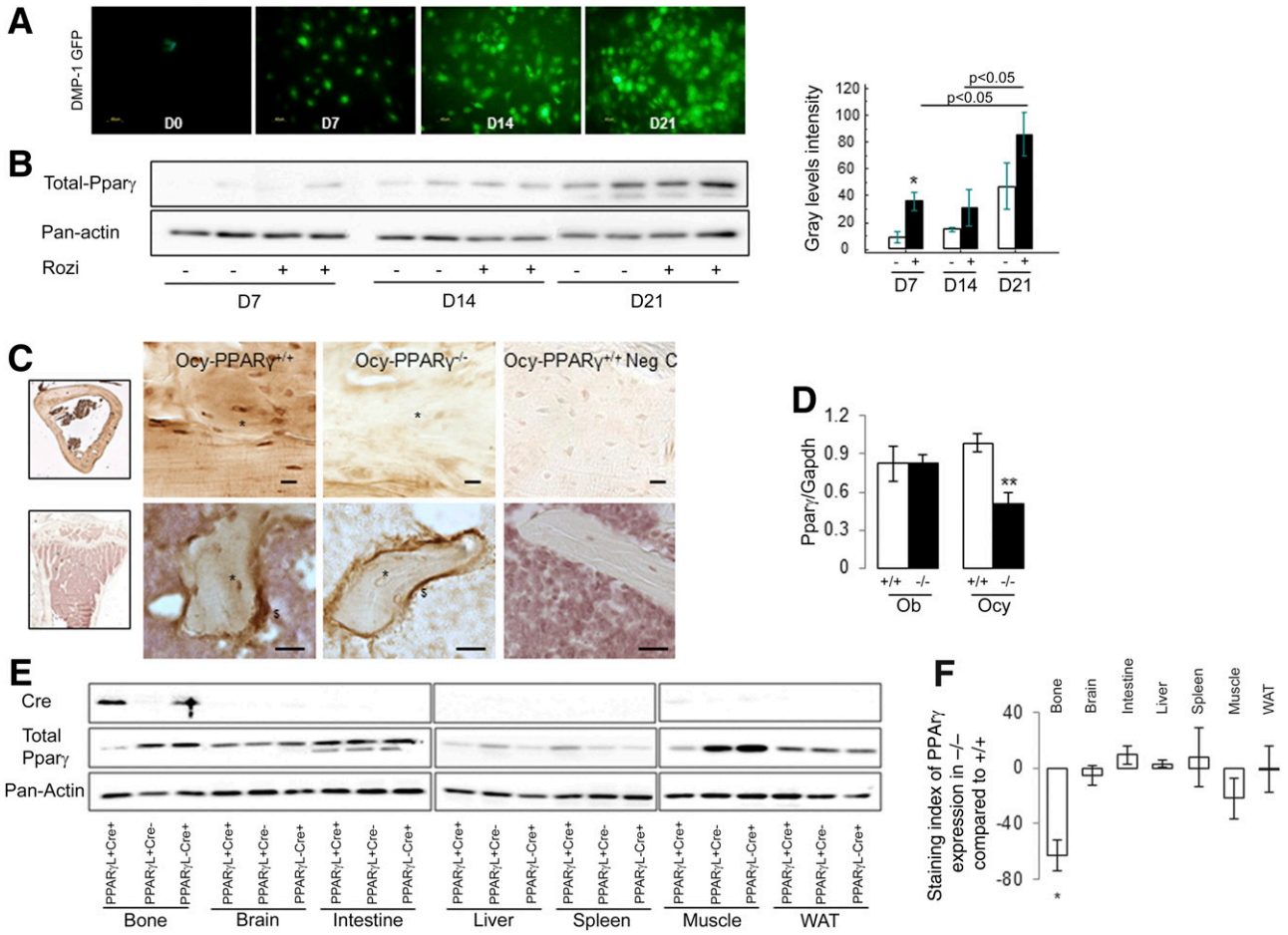

Figure 1—PPARγ expression in IDG-W3 osteocyte cell lines and specific deletion of PPARγ in osteocyte using DMP1-cre promotor. *A*: Time course expression of Dmp1 in IDG-W3 osteocyte cell line mark with GFP under Dmp1 promoter. D, day. (n = 3). *B*: Time course expression of PPARγ in IDG-W3 osteocyte cells treated or not with rosiglitazone (Rozi) (n = 3). *C*: Immunohistochemical staining of PPARγ in cross-sectional tibia at the midshaft (upper panel, bar = 20 μm) and in longitudinal sections of the proximal tibia (lower panel, bar = 40 μm) showing the absence of staining in osteocytes of the cortical and trabecular compartments (*), whereas the staining remains in osteoclasts ($) ($n$ = 4). *D*: PPARγ expression in the bone fractions of *Ocy-PPARγ*$^{-/-}$ and *Ocy-PPARγ*$^{+/+}$ mice (n = 4). *E*: Western blot of Dmp1-Cre, total PPARγ, and Pan actin (n = 3). *F*: Western blot quantification by ImageJ of PPARγ protein expression in *Ocy-PPARγ*$^{-/-}$ reported to *Ocy-PPARγ*$^{+/+}$ (n = 3). Bars show means (±SEM). Closed bars, *Ocy-PPARγ*$^{-/-}$; open bars, *Ocy-PPARγ*$^{+/+}$. *P < 0.05, **P < 0.01, significant difference vs. *Ocy-PPARγ*$^{+/+}$.

mainly during the night (Fig. 3*G* and *H*); these differences remained significant after division by lean mass or by performance of an ANCOVA (Supplementary Fig. 3*A*–*D*). Movement and cumulative food intake were unchanged (Supplementary Fig. 4*A* and *B*). RER was significantly higher in Ocy-PPARγ$^{-/-}$ compared with Ocy-PPARγ$^{+/+}$ (0.91 ± 0.008 vs. 0.86 ± 0.01, $P < 0.01$), with values indicating a mix of fat and carbohydrate as fuel sources. In order to further investigate the higher energy expenditure of Ocy-PPARγ$^{-/-}$, we evaluated the body temperature of different regions of interest. Internal body temperature, i.e., eye temperature measurement, and temperature in the musculoskeletal limb were higher in Ocy-PPARγ$^{-/-}$ compared with Ocy-PPARγ$^{+/+}$ mice (Fig. 3*I*). Analyses of the ventral and dorsal infrared images showed that the interscapular regions, i.e., brown adipose tissue (BAT), contributed to the overall higher temperature in Ocy-PPARγ$^{-/-}$ compared with inguinal fat, i.e., white adipose tissue (WAT) (Fig. 3*I*). However, body temperature response to 24 h cold exposure was similar between genotypes (Supplementary Fig. 4*C*). To further address the metabolic effects of PPARγ deletion in OB-OCY, we performed a hyperinsulinemic-euglycemic clamp in conscious and unrestrained mice. Ocy-PPARγ$^{-/-}$ mice exhibited a marked increase in the glucose infusion rates needed to maintain the clamped glucose levels, demonstrating an increase of insulin sensitivity (Fig. 3*J*). In accordance, insulin staining in the pancreas showed smaller islet size in Ocy-PPARγ$^{-/-}$ compared with Ocy-PPARγ$^{+/+}$, whereas the number remained unchanged (Supplementary Fig. 4*D*–*G*). Moreover, phosphorylation level of Akt^{ser473}, considered an important downstream target of insulin signaling, was significantly higher in bone, skeletal muscle, BAT, and liver in

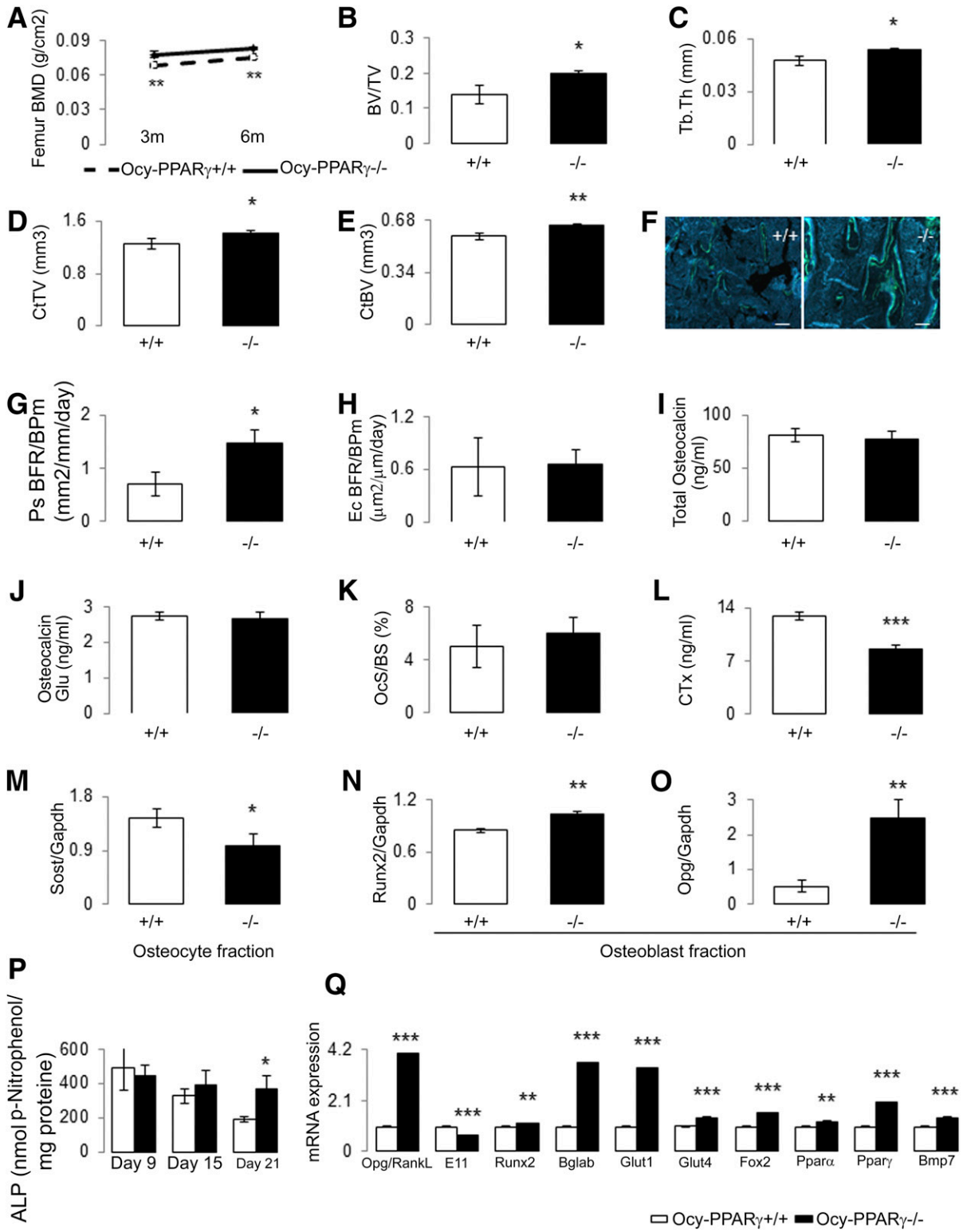

Figure 2—Bone phenotype of PPARγ-deficient mice in late OB-OCY at 6 months of age. *A*: Femoral BMD. *B* and *C*: BV/TV and trabecular thickness (Tb.Th) at the distal femur. *D* and *E*: Ct.TV and Ct.BV at midshaft femur (n = 8 per group). *F*: Images illustrate double fluorescent calcein labels on trabecular surfaces (n = 6 per group; bar = 50 µm). *G* and *H*: Bone formation indices at periosteal (Ps) and endocortical (Ec) surfaces. BFR and bone perimeter (BPm) (n = 6 per group). *I* and *J*: Total and undercarboxylated osteocalcin (osteocalcin glu) measured by ELISA in serums. *K*: Osteoclast surface on bone surface (OcS/BS) (n = 8 per group). *L*: Serum collagen type I crosslinked C-telopeptide (CTX) measured by ELISA assay in serums. *M*–*O*: Relative mRNA gene expression from flushed femur after isolation of osteocyte fraction (*M*) and osteoblast fraction (*N* and *O*) (n = 4 per group). *P*: Alkaline phosphatase (ALP) production in mesenchymal stem cell after 9, 15, or 21 days of culture in osteogenic condition (n = 4 per group). *Q*: Relative mRNA gene expression after 21 days of cultures from *Ocy-PPARγ*$^{-/-}$ and *Ocy-PPARγ*$^{+/+}$ femurs (n = 4 per group). Bars show means (±SEM). *P < 0.05, **P < 0.01, ***P < 0.001 significant difference vs. Ocy-PPARγ$^{+/+}$.

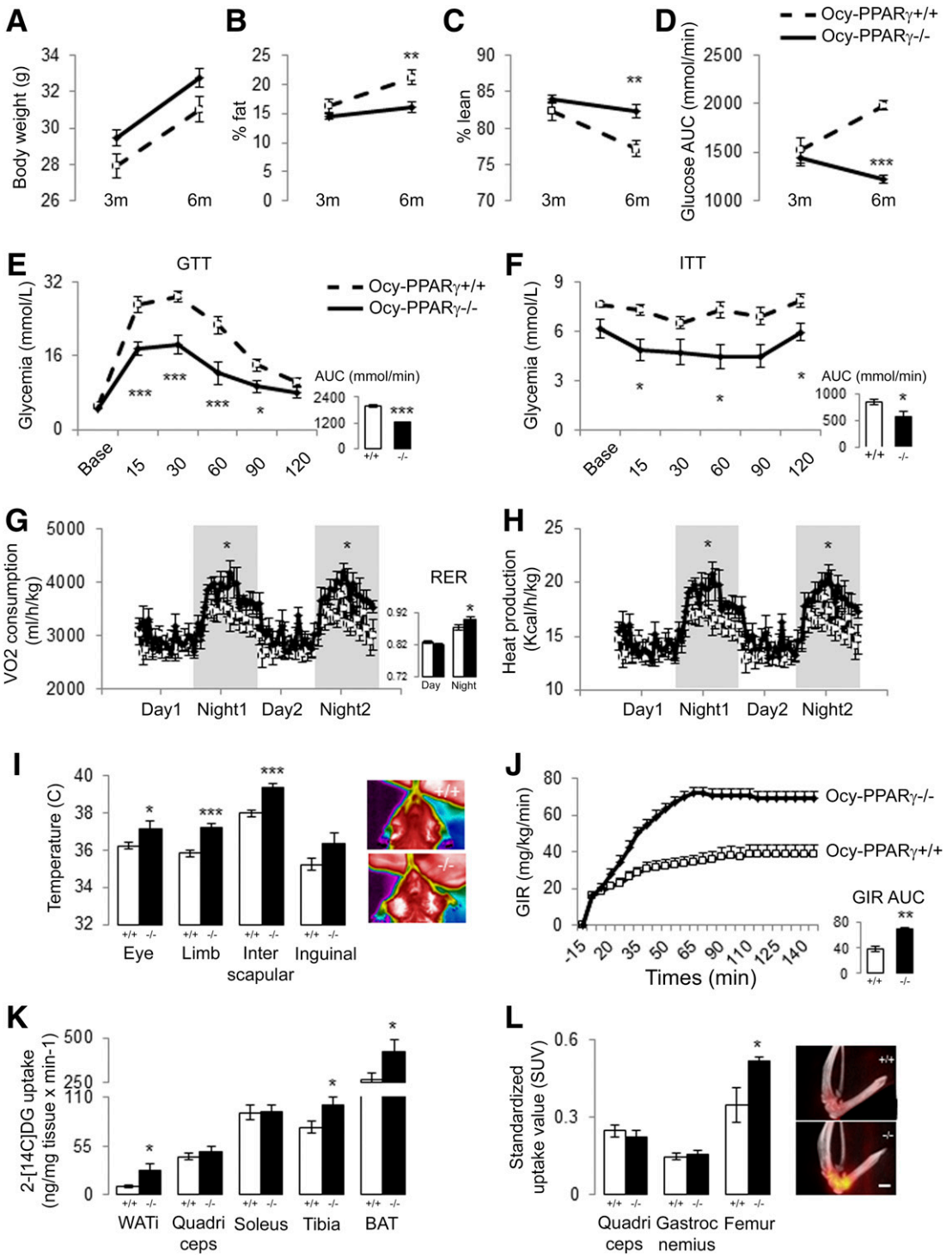

Figure 3—At 6 months of age, PPARγ deletion in late osteoblast/osteocyte controls glucose homeostasis by increasing metabolic rate and glucose uptake in WAT, BAT, and bone and improves insulin sensitivity. *A–C*: Body composition analyzed in vivo by PIXImus; body weight (*A*), fat mass percentage (%) (*B*), and lean mass percentage (*C*) ($n = 8$ per group). *D*: Glucose AUC obtained during a GTT ($n = 8$ per group). *E*: GTT at 6 months ($n = 8$ per group). *F*: ITT ($n = 8$ per group). *G* and *H*: Energy metabolism investigation performed in metabolic cages during two consecutive days and nights ($n = 6$ per group); VO_2 and AUC of RER (*G*) and heat production (*H*). *I*: Body temperature evaluated by infrared camera. Note the higher temperature of the limb of *Ocy-PPARγ*$^{-/-}$, indicated by the white spots ($n = 8$ per group). *J* and *K*: Glucose infusion rate (GIR) and tissue-specific 2-[14C]deoxyglucose (2-[14C]DG) in iWAT and BAT during hyperinsulinemic-euglycemic clamp in awake mice ($n = 6$ per group). *L*: Standardized uptake values (SUVs) of the radiolabeled tracer 18FDG; note the higher 18FDG uptake in bone of the limb of *Ocy-PPARγ*$^{-/-}$, indicated by yellow spots ($n = 4$–5 per group; bar = 1 mm). Bars show means (±SEM). Closed bars or continuous lines, *Ocy-PPARγ*$^{-/-}$; open bars or dashed lines, *Ocy-PPARγ*$^{+/+}$. *$P < 0.05$, **$P < 0.01$, ***$P < 0.001$ significant difference vs. *Ocy-PPARγ*$^{+/+}$.

Ocy-PPARγ$^{-/-}$ compared with Ocy-PPARγ$^{+/+}$ mice and tended to be in WAT (Supplementary Fig. 4*H* and *I*). To investigate peripheral glucose uptake, we coadministered 2-[^{14}C]deoxyglucose during the clamp. Whereas no changes were observed in skeletal muscle, there was an increased uptake from the inguinal (i)WAT, the tibia, and BAT in Ocy-PPARγ$^{-/-}$ compared with Ocy-PPARγ$^{+/+}$ mice (Fig. 3*K*). These results were confirmed by microPET, resulting in more accumulation of fluodeoxyglucose (^{18}F) (18FDG) in long bones of Ocy-PPARγ$^{-/-}$ (Fig. 3*L*), whereas no significant differences were observed in quadriceps and gastrocnemius.

Lack of PPARγ in Mature OB-OCY Increased Adipose Browning

We next investigated whether the higher consumption of glucose by adipose tissue originated from a difference in adipocyte density and volume. Measuring adipocyte size distribution revealed an increased number of small adipocytes and a decreased number of large adipocytes in eWAT of Ocy-PPARγ$^{-/-}$ (Fig. 4*A* and *B*). Moreover, morphologically, white fat depots had more of a multinodular phenotype in Ocy-PPARγ$^{-/-}$ compared with Ocy-PPARγ$^{+/+}$ mice (Fig. 4*A*). These features are characteristic of beige adipocyte formation within WAT as well as mitochondrial activity of BAT. Immunohistochemistry confirmed the expression of uncoupling protein 1 (UCP1) in WAT of Ocy-PPARγ$^{-/-}$ but not in Ocy-PPARγ$^{+/+}$ (Fig. 4*A* and *B*). In BAT depots, we observed dense UCP1 staining in both genotypes; however, larger white droplets accumulated in the BAT depots in Ocy-PPARγ$^{+/+}$ (Fig. 4*C*). Fat depots of the Ocy-PPARγ$^{-/-}$ mice showed increased expression of brown adipocyte–specific markers compared with Ocy-PPARγ$^{+/+}$, particularly in inguinal WAT (Fig. 4*D–F*). In vitro, primary BAT cultures showed larger numbers of lipid droplets in Ocy-PPARγ$^{-/-}$, with a smaller size than in Ocy-PPARγ$^{+/+}$ (Fig. 4*G*). BAT and inguinal WAT primary culture also confirmed darker UCP1 staining in Ocy-PPARγ$^{-/-}$ compared with Ocy-PPARγ$^{+/+}$

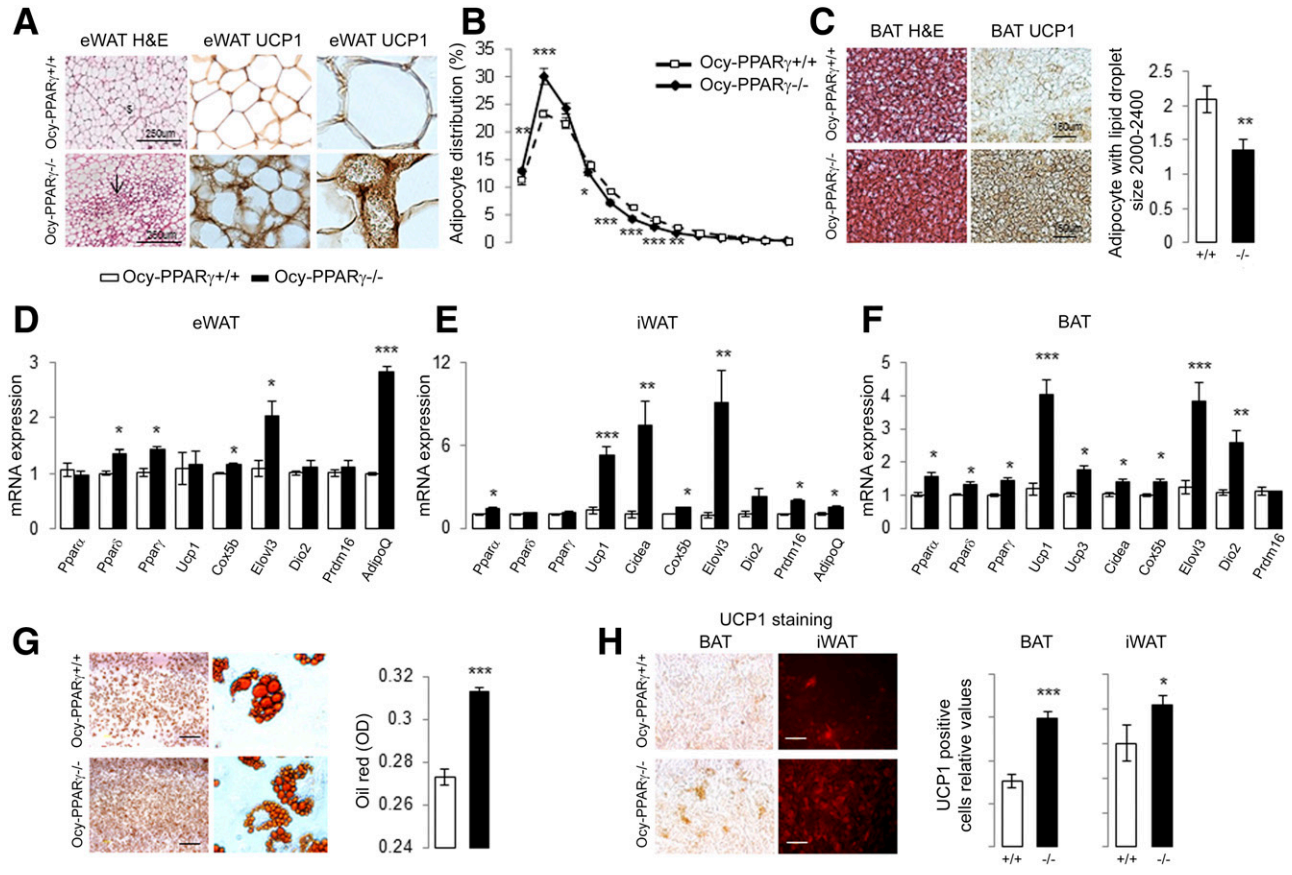

Figure 4—At 6 months of age, PPARγ deletion in mature OB-OCY promotes browning of the WAT and BAT activity. *A*: Hematoxylin-eosin (H&E) and UCP1 staining on sections from eWAT. Arrows indicate accumulation of small lipid droplets. $More brown staining in *Ocy-PPARγ*$^{-/-}$ vs. *Ocy-PPARγ*$^{+/+}$ (n = 6 per group). *B*: Cell-size profiling of adipocytes from eWAT; points show mean of pooled fractions from each animal (n = 6 per group with 4 sections per animals). *C*: Hematoxylin-eosin and UCP1 staining on sections from BAT (n = 6 per group with 3 sections per animals). *D–F*: Relative mRNA gene expression in eWAT (*D*), iWAT (*E*), and BAT (*F*) (n = 4 per group). *G*: Primary culture of BAT; Oil Red O staining after 6 days of culture indicated larger numbers of small lipid droplets (n = 6 per group; bar = 100 μm). *H*: Immunohistochemistry on BAT and iWAT, automated quantification of UCP1 (n = 4 per group; bar = 100 μm). Bars show mean (±SEM). OD, optical density. *P < 0.05, **P < 0.01, ***P < 0.001 significant difference vs. *Ocy-PPARγ*$^{+/+}$.

(Fig. 4*H*), thus arguing a browning of WAT and more activity of BAT in Ocy-PPARγ$^{-/-}$ mice.

Ocy-PPARγ$^{-/-}$ Mice Partially Protected Against the Dysmetabolism Induced by High Dietary Fat Intake

We next challenged the Ocy-PPARγ$^{-/-}$ mice to an HFD or control diet (CD) to investigate whether these mice are protected against diet-induced bone fragility, obesity, and hyperglycemia. In Ocy-PPARγ$^{+/+}$ mice, HFD did not affect endocortical bone formation rate but increased periosteal BFR, perhaps as a result of body weight increase (Supplementary Fig. 5*A* and *B*). Ocy-PPARγ$^{-/-}$ mice on HFD exhibited a higher endocortical bone formation rate than Ocy-PPARγ$^{+/+}$ (Supplementary Fig. 5*B*). Hence, Ocy-PPARγ$^{-/-}$ HFD mice have more cortical bone volume on tissue volume (Ct. BV/TV) and cortical thickness (Ct.Th) than Ocy-PPARγ$^{+/+}$ mice (Supplementary Fig. 5*C*–*E*). After biomechanical strength testing using a three-point bending test, we observed that Ocy-PPARγ$^{-/-}$ mice exhibited more ultimate force, stiffness, and plastic and fracture energy compared with Ocy-PPARγ$^{+/+}$ (Supplementary Table 4). In Ocy-PPARγ$^{+/+}$ mice, HFD increased elastic and decreased plastic energy, whereas Ocy-PPARγ$^{-/-}$ mice were unaffected by HFD (Supplementary Table 4). An HFD regimen increased body weight in both genotypes over time (Fig. 5*A*). However, food and hydric recording over 24 h indicated more intake in Ocy-PPARγ$^{-/-}$ compared with Ocy-PPARγ$^{+/+}$ mice (Supplementary Fig. 6*A* and *B*). Nevertheless, the final body weight observed in Ocy-PPARγ$^{-/-}$ did not reach the values of Ocy-PPARγ$^{+/+}$ mice, suggesting that Ocy-PPARγ$^{-/-}$ animals were partially protected from HFD (Fig. 5*A*). EchoMRI scans after 8 weeks of HFD showed that fat mass increase was prevented in Ocy-PPARγ$^{-/-}$ (increase of 17% vs. CD and 44% vs. CD in Ocy-PPARγ$^{+/+}$, $P < 0.05$), whereas lean mass was greater (14.2% vs. CD and 9.6% vs. CD in Ocy-PPARγ$^{+/+}$) (Fig. 5*B* and *C*). On HFD, movement, VO_2, and heat were increased in Ocy-PPARγ$^{-/-}$ (41%, 13%, and 13% vs. Ocy-PPARγ$^{+/+}$, $P < 0.05$) (Fig. 5*D*–*F*) compared with the CD experiment; genotype differences on HFD disappeared after division of parameters per lean mass or ANCOVA analysis (Supplementary Fig. 6*C*–*F*). RER was not significantly different between genotypes and mean value decreased compared with CD, indicating that fat is the predominant fuel source (Supplementary Fig. 6*G*). Body temperature was also higher, particularly in the BAT neck region (1.5% vs. Ocy-PPARγ$^{+/+}$, $P < 0.01$) (Supplementary Fig. 7*A*). Responses to GTT, ITT, and PTT were improved in Ocy-PPARγ$^{-/-}$ (AUC −22%, −9%, and −13%, respectively, vs. Ocy-PPARγ$^{+/+}$, $P < 0.1$) (Fig. 5*G*–*I*). To further address the metabolic effects of PPARγ deletion in OB-OCY, we performed a hyperinsulinemic-euglycemic clamp after 8 weeks of the dietary challenge. Ocy-PPARγ$^{-/-}$ mice exhibited the same trend of a higher glucose infusion rate required to maintain the clamped glucose levels, demonstrating an increase of insulin sensitivity (Fig. 5*J*). Measurement of insulin levels before and after clamping confirmed the increase in insulin levels during clamping and illustrated no significant difference between genotypes (Supplementary Fig. 7*B*). The difference between glucose disappearance (R_d) before and after the clamp was higher in Ocy-PPARγ$^{-/-}$ mice, suggesting less hepatic glucose production (Supplementary Fig. 7*C*). We coadministered 2-[^{14}C]deoxyglucose during the clamp. No changes were observed in glucose uptake in skeletal muscle and WAT, although there was a significant increased uptake by the tibia and a trend for the BAT in Ocy-PPARγ$^{-/-}$ compared with Ocy-PPARγ$^{+/+}$ mice (Supplementary Fig. 7*D*). These results were confirmed by microPET, with more accumulation of 18FDG in BAT and in the long bones of Ocy-PPARγ$^{-/-}$ (Fig. 5*K* and *L*).

Lack of PPARγ in Late OB-OCY Prevented Fat Infiltration in Skeletal Muscle and Liver and Increased Adipose Browning

On CD, histology of the gastrocnemius revealed homogenous fiber size distribution, polygonal shape of fibers, and number of peripheral nuclei in both genotypes (Fig. 6*A*). On HFD, Ocy-PPARγ$^{-/-}$ seemingly prevented fibrosis in the tissue, with less mononucleated inflammatory cells, central nucleation of the myofibers, and fat infiltration compared with Ocy-PPARγ$^{+/+}$ mice. In accordance, gene expression analysis in HFD showed more muscle regeneration and fatty acid (FA) oxidation, indicated by high expression of Mef2b and PPARα/δ, and muscle force in Ocy-PPARγ$^{-/-}$ (Fig. 6*B* and *C*). Liver steatosis, as illustrated by accumulation of white lipid droplets stained with Oil Red O, was less pronounced in Ocy-PPARγ$^{-/-}$ compared with Ocy-PPARγ$^{+/+}$ on HFD (Fig. 6*D*). Gene expression indicated reduced FA transporters in Ocy-PPARγ$^{-/-}$, in particular Cd36, which was confirmed by Western blot (Fig. 6*E* and *F*), suggesting a reduced uptake of FA from the bloodstream into the liver. Moreover, it also indicated less lipogenesis in Ocy-PPARγ$^{-/-}$ through the lower expression of Fas, Acc1, and Acc2 and a decrease in gluconeogenesis through a decrease in Ppeck expression (Fig. 6*E*). FA oxidation, export and cholesterol were modestly affected (Supplementary Fig. 7*E*). Adipocyte morphology and beige adipogenic gene markers including Ucp1, Cox5b, and Dio2 indicated a browning of the eWAT in Ocy-PPARγ$^{-/-}$ (Fig. 6*G*). Furthermore, in the BAT, Ocy-PPARγ$^{-/-}$ exhibited less large droplet accumulation compared with Ocy-PPARγ$^{+/+}$ on HFD (adipocyte with lipid droplet size 2,000–2,400; 5.3 ± 0.2% compared with 8.3 ± 0.5%, respectively, $P < 0.01$). Gene expression analysis showed more capability of lipid oxidation in Ocy-PPARγ$^{-/-}$ versus Ocy-PPARγ$^{+/+}$ through the increased expression of PPARα/δ/γ, Elovl3, Dio2, Ucp1, and Lpl (Fig. 6*H*).

Osteokines Secreted by Ocy-PPARγ$^{-/-}$ Mice Control Adipose, Liver, and Pancreas Functions

To investigate the proof of concept that deletion of PPARγ in bone cells is able to prevent hepatic steatosis, improve FA metabolism by adipocytes, and augment pancreatic islet insulin secretion, we applied CM or performed real cocultures of mature osteoblasts with hepatocytes, adipocytes,

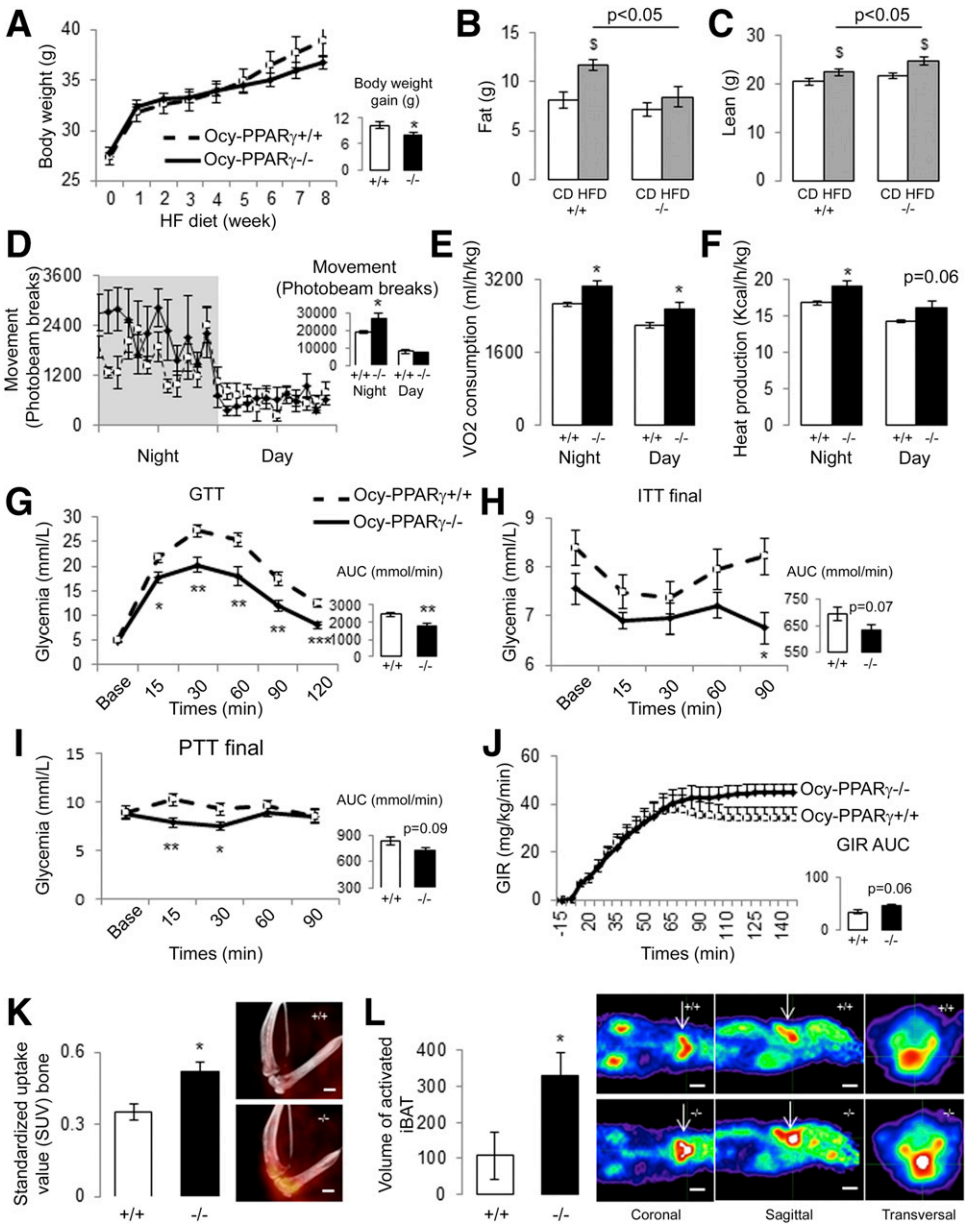

Figure 5—PPARγ deletion in late OB-OCY improves glucose homeostasis by increasing metabolic rate and improving insulin sensitivity and glucose uptake by BAT and bone after 8 weeks of HFD. *A*: Body weight (n = 8 per group). *B* and *C*: Fat and lean mass evaluated by echoMRI (n = 8 per group); $\$P < 0.05$ significant difference vs. chow diet. From *D* to *L*, all the mice are on HFD. *D–F*: Energy metabolism investigation performed in metabolic cages during 1 day and night (n = 6 per group); movement (*D*), VO_2 (*E*), heat production (*F*). *G*: GTT (n = 8 per group). *H*: ITT (n = 8 per group). *I*: PTT (n = 8 per group). *J*: Glucose infusion rate (GIR) during hyperinsulinemic-euglycemic clamp in awake mice (n = 6 per group). *K* and *L*: Standardized uptake values (SUV) of the radiolabeled tracer 18FDG in bone (bar = 1 mm) and BAT (bar = 1 cm); note the higher 18FDG uptake in bone and BAT of *Ocy-PPARγ*$^{-/-}$ indicated by red and white spots (n = 5 per group). Arrows indicate 18FDG uptake in the BAT. Bars show means (±SEM). HF, high-fat. $^*P < 0.05$, $^{**}P < 0.01$, $^{***}P < 0.001$ significant difference vs. *Ocy-PPARγ*$^{+/+}$.

and pancreatic β-cells. For this purpose, primary OB-OCY of *Ocy-PPARγ*$^{-/-}$ and *Ocy-PPARγ*$^{+/+}$ were extracted from long bones as previously described (22). After 21 days of culture, CM was collected and added to primary hepatocytes from WT mice incubated with a mix of oleate and palmitate for 48 h to induce steatosis (Fig. 7*A*). Lipid content in CM of *Ocy-PPARγ*$^{+/+}$ and *Ocy-PPARγ*$^{-/-}$ OB-OCY was not detectable, arguing a similar exposure of lipid on hepatocytes. The effects on lipid metabolism were analyzed by gene expression and Oil Red O staining. Lipid droplet accumulation was lesser in hepatocytes exposed to *Ocy-PPARγ*$^{-/-}$ versus *Ocy-PPARγ*$^{+/+}$ CM (Fig. 7*B*). *Cd36* FA transporter expression was also lower with *Ocy-PPARγ*$^{-/-}$ CM (−51% vs. no control media and −52% vs. *Ocy-PPARγ*$^{+/+}$ CM, all $P < 0.001$), and *Pparα* gene expression was higher (48% vs. control media and 22% vs. *Ocy-PPARγ*$^{+/+}$ CM, all $P < 0.05$) (Fig. 7*C*). We then tested the effect of CM on 3T3L1 adipocyte cell lines. Exposure to *Ocy-PPARγ*$^{-/-}$ CM

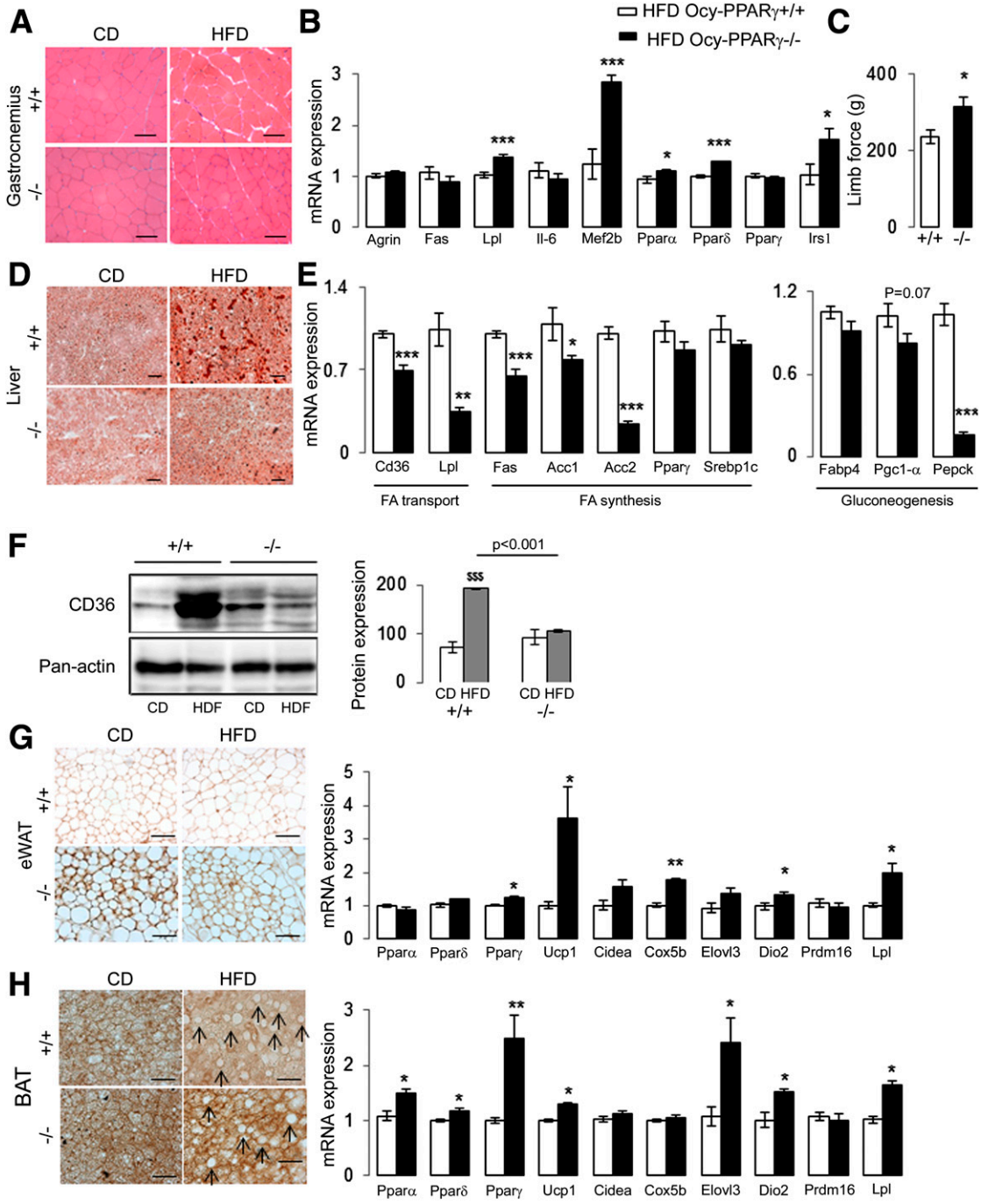

Figure 6—PPARγ deletion in late OB-OCY prevents fat infiltration in skeletal muscle and steatosis and improves browning and BAT activity after 8 weeks of HFD. *A*: Hematoxylin-eosin staining on sections of gastrocnemius (n = 6 per group with 3 sections per animals; bar = 40 μm). *B*: Relative mRNA gene expression for HFD in gastrocnemius (n = 4 per group). *C*: Limb force evaluated by handgrip for HFD groups (n = 8 per group). *D*: Oil Red O staining on sections of liver; note the larger accumulation of lipid droplets in *Ocy-PPARγ*$^{+/+}$ vs. *Ocy-PPARγ*$^{-/-}$ (n = 6 per group; bar = 50 μm). *E*: Relative mRNA gene expression of FA transports, FA synthesis, and gluconeogenesis markers in liver on HFD (n = 4 per group). *F*: Western blot of CD36 and quantification for CD and HFD (n = 3 per group). $$$$P$ < 0.001 significant difference vs. CD. *G*: UCP1 staining on sections from eWAT and relative mRNA gene expression for HFD (n = 6 per group with 3 sections per animals; bar = 100 μm). *H*: UCP1 staining on sections from BAT; arrows indicate less accumulation of big lipid droplets in BAT of *Ocy-PPARγ*$^{-/-}$ vs. *Ocy-PPARγ*$^{+/+}$ and relative mRNA gene expression for HFD (n = 6 per group with 3 sections per animals; bar = 100 μm). Bars show means (±SEM). Black bars, *Ocy-PPARγ*$^{-/-}$; white bars, *Ocy-PPARγ*$^{+/+}$. *P < 0.05, **P < 0.01, ***P < 0.001 significant difference vs. *Ocy-PPARγ*$^{+/+}$.

improved lipid metabolism as shown by Oil Red O quantification, and the gene expression profile was similar to the one described in vivo with an increase of FA synthesis and oxidation, respectively, illustrated by an increase in lipoprotein lipase, *Fas*, and *Pparα/δ/γ* (Fig. 7*D*). Immunostaining and Western blot analysis indicated an increased expression

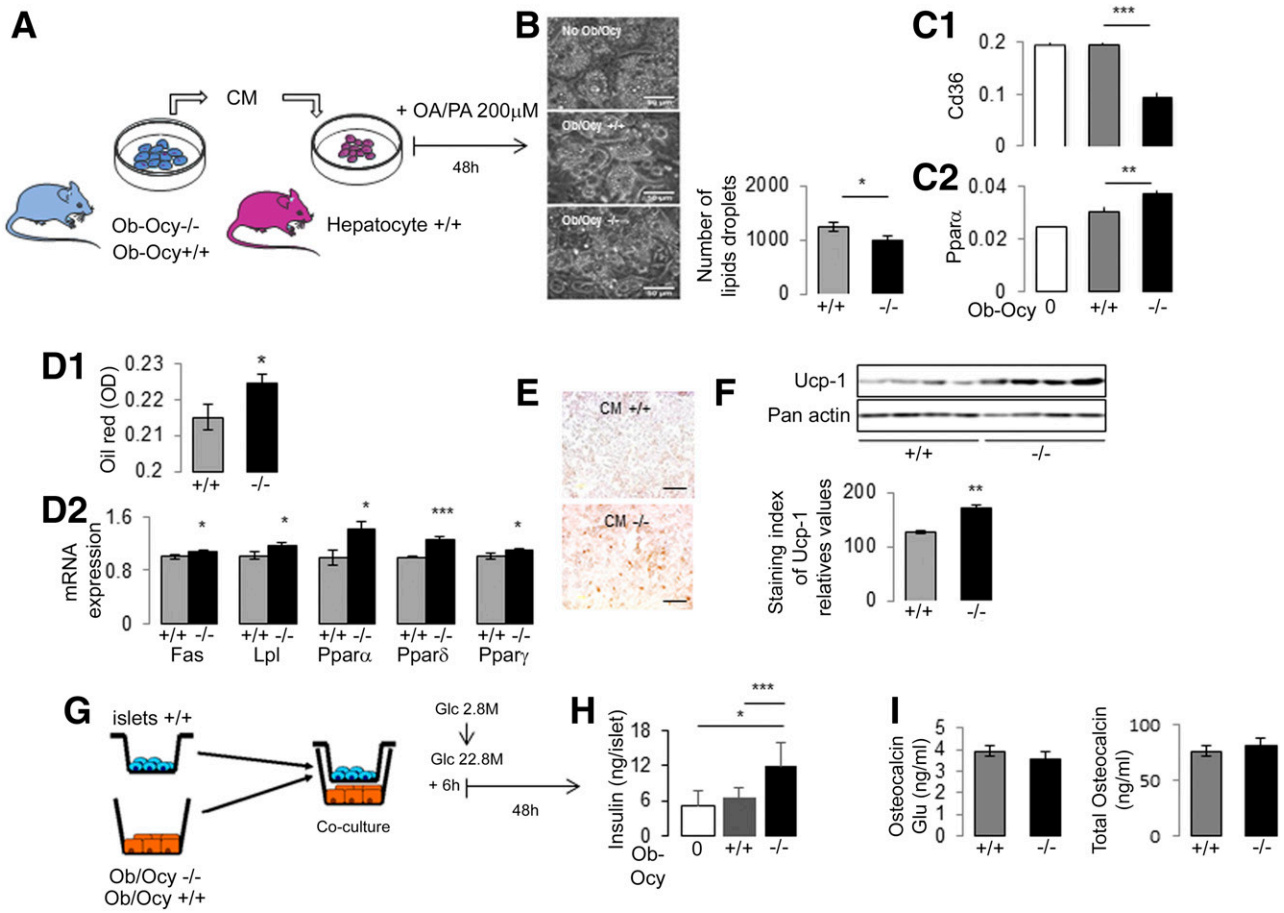

Figure 7—OB-OCY secrete a factor regulating steatosis, lipid oxidation, and insulin secretion. *A*: Schematic of the experiment performed on primary hepatocyte. *B*: Images illustrating less lipid droplets in hepatocytes exposed to *Ocy-PPARγ*$^{-/-}$ OB-OCY CM (n = 3 per group, duplicate experiment). Bar = 50 μM. *C*: Relative mRNA gene expression of CD36 transporter (*C1*) and PPARα (*C2*) (n = 4 per group, duplicate experiment). *D–F*: Effects of 6 days of *Ocy-PPARγ*$^{-/-}$ CM on 3T3L1 cell line differentiation in adipocytes (n = 6 per group, duplicate experiment). Oil Red O quantification (*D1*), relative mRNA gene expression (n = 4 per group, duplicate experiment) (*D2*), UCP1immunostaining (n = 4 per group, bar = 100 μm) (*E*), and Western blot of UCP1 (n = 4 per condition) (*F*). *G*: Schematic of the coculture performed between late OB-OCY and isolated islets (n = 8–10 per group, duplicate experiment). *H*: Insulin released from cocultured islets stimulated with 28 mmol/L glucose (n = 8–13 per group). *I*: Total and undercarboxylated osteocalcin (osteocalcin glu) measured by ELISA in CM (n = 10 per group). Bars show means (±SEM). Black bars, *Ocy-PPARγ*$^{-/-}$; white bars, CM of the original cell (hepatocyte, adipocyte, or islet); dark-gray bars, *Ocy-PPARγ*$^{+/+}$. OA/PA, oleic acid/palmitic acid. OD, optical density. *P < 0.05, **P < 0.01, ***P < 0.001 significant difference.

of UCP1 in cells exposed to *Ocy-PPARγ*$^{-/-}$ CM compared with WT. Coculture of mature OB-OCY *Ocy-PPARγ*$^{-/-}$ was also performed with pancreatic islets isolated from *Ocy-PPARγ*$^{+/+}$ mice, in the presence of stimulatory glucose (28 mmol/L) for 6 h. Insulin release was quantified by radioimmunoassay. Coculture with OB-OCY *Ocy-PPARγ*$^{-/-}$ increased insulin secretion by pancreatic islets (130% vs. no OB and 83% vs. OB-OCY *Ocy-PPARγ*$^{+/+}$, both $P < 0.01$) (Fig. 7*G* and *H*). In order to confirm that these effects were independent of osteocalcin, as shown in vivo, we evaluated total and decarboxylated osteocalcin in CM of OB-OCY *Ocy-PPARγ*$^{-/-}$ and *Ocy-PPARγ*$^{+/+}$; no differences were observed (Fig. 7*I*). Based on literature and gene expression profiles (Fig. 2*Q*), we analyzed BMP7 levels in the CM and serum of the aging experiment by ELISA assay and observed higher levels in *Ocy-Pparγ*$^{-/-}$ (respectively, 8.4% and 107% vs. *Ocy-Pparγ*$^{+/+}$, $P < 0.05$) (Fig. 8*A* and *B*). In turn, the addition of BMP7-neutralizing antibody to *Ocy-Pparγ*$^{-/-}$ CM blocked the steatosis prevention in hepatocytes (Fig. 8*C* and *D*) and FA oxidation in 3t3L1 adipocytes (Fig. 8*E* and *F*). Moreover, when we added recombinant BMP7 to *Ocy-Pparγ*$^{+/+}$ CM, we partially simulated the effect of *Ocy-Pparγ*$^{-/-}$ CM with an increase in Oil Red O staining and *Pparδ/γ* gene expression (Fig. 8*G* and *H*). Finally, in vivo administration of a BMP7-neutralizing antibody blocked the hypoglycemia described in *Ocy-Pparγ*$^{-/-}$ mice (Fig. 8*I*).

DISCUSSION

PPARγ is a master transcriptional factor that is expressed in many tissues, playing both common and specific roles wherever it is expressed. Here we show that PPARγ in bone and more specifically in mature OB-OCY acts as a mediator of systemic energy metabolism and coregulates bone and glucose homeostasis. PPARγ deletion results in an increase

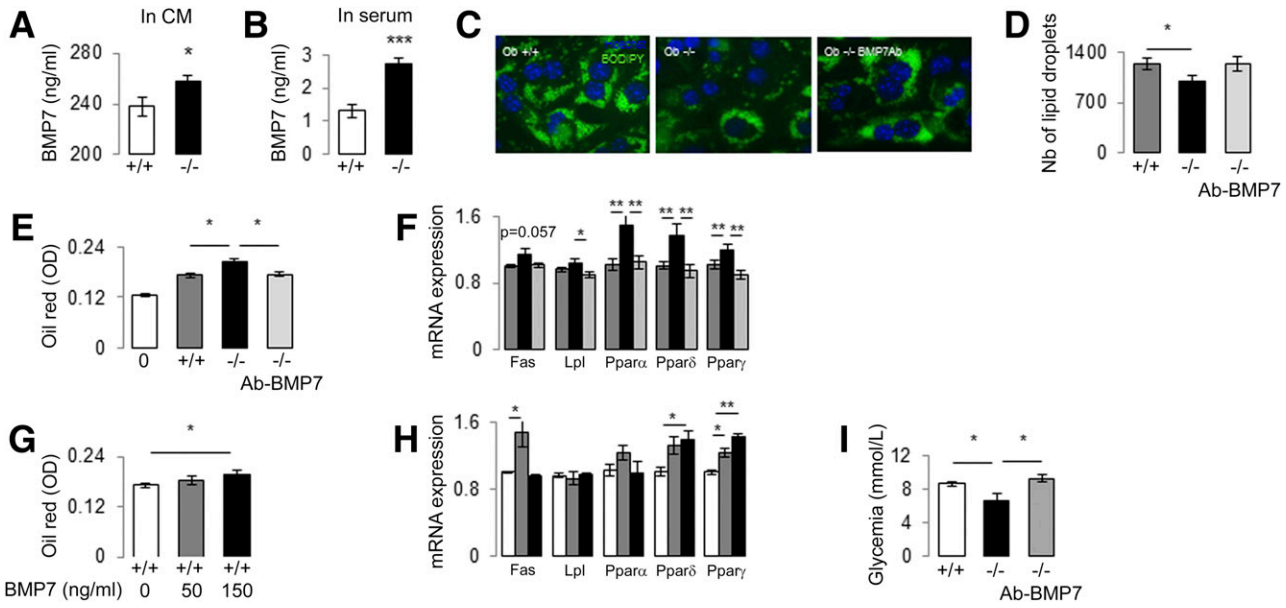

Figure 8—OB-OCY secrete BMP7, regulating steatosis and lipid oxidation, respectively, in hepatocyte and adipocyte. *A* and *B*: BMP7 measured by ELISA assay in CM and serum of *Ocy-PPARγ*$^{-/-}$ and *Ocy-PPARγ*$^{+/+}$ mice aged 6 months. *C* and *D*: Images and quantification of lipid droplets in hepatocytes exposed to *Ocy-PPARγ*$^{+/+}$ CM, *Ocy-PPARγ*$^{-/-}$ CM, and *Ocy-PPARγ*$^{-/-}$ CM with or without BMP7-neutralizing antibody (Ab-BMP7) (n = 3 per group, duplicate experiment). Nb, number. *E* and *F*: Oil Red O quantification in 3T3L1 cell lines after 6 days of exposure to *Ocy-PPARγ*$^{+/+}$, *Ocy-PPARγ*$^{-/-}$, and *Ocy-PPARγ*$^{-/-}$ CM ± Ab-BMP7. *F*: Relative mRNA gene expression. *G* and *H*: Oil Red O quantification in 3T3L1 cell lines after 6 days of exposure to *Ocy-PPARγ*$^{+/+}$ CM with or without two doses of recombinant BMP7 (50 and 150 ng/mL). *H*: Relative mRNA gene expression. *I*: Glucose levels after two intravenous injections of Ab-BMP7 (273 ng/30 g body wt every 2 days) as previously described (38). Glucose was evaluated 6 h after the last injections. Bars show means (±SEM). Black bars, Ocy-Pparγ$^{-/-}$; white bars, CM of the original cell (hepatocyte, adipocyte, or islet); dark-gray bars, Ocy-Pparγ$^{+/+}$; light-gray bars, Ocy-Pparγ$^{-/-}$ plus BMP7-neutralizing antibody. OD, optical density. *P < 0.05, **P < 0.01, ***P < 0.001 significant difference.

in bone formation and a decrease in bone resorption during bone mass acquisition, thereby increasing BMD in young-adult rodents. In accordance with the pharmacological work of Marciano et al. (29), repression of PPARγ promotes osteogenesis in part through the increased production and secretion of members of the bone morphogenetic protein family. These effects are opposite those of PPARγ activators, such as thiazolidinediones, which inhibit bone formation and promote osteocyte apoptosis through an increase in sclerostin expression, a Wnt antagonist (30,31). Despite the increase in bone formation index, both total and decarboxylated osteocalcin were unchanged in the serums. Inhibition of PPARγ decreased the bone resorption marker, CTX, through an increased *Opg/RankL* ratio, supporting the notion that PPARγ inhibition in osteocytes is able to orchestrate an uncoupling effect in bone. Interestingly, the comparative increase in BMD, trabecular and cortical microarchitecture, and bone strength in *Ocy-PPARγ*$^{-/-}$ mice acquired from an early age remained throughout aging. Our study meaningfully highlights the important role played by PPARγ in Dmp1-expressing cells, predominantly osteocytes, contrasting with the absence of a drastic phenotype in the PPARγ-flox col3.6-cre mice (3). In addition to the bone phenotype, mice deficient for PPARγ in Dmp-1–expressing cells had improved body composition at 6 months of age, gained less fat, and lost less lean mass. They exhibited a high RER and metabolic rate independently of lean mass. Strikingly, body temperature was higher, particularly in the BAT-rich neck region and musculoskeletal limb region, showing that deletion of PPARγ in bone improved thermogenic capacity without changing tbone response to acute cold exposure. In addition, WAT was clearly being converted to BAT (known as beige), a mechanism well known to reduce obesity and hyperglycemia (28). 2-[14C]deoxyglucose and 18FDG distributions indicated more glucose consumption in the bone and BAT of *Ocy-PPARγ*$^{-/-}$ mice as a result of an increase in insulin sensitivity. Given that the difference in glucose levels during the GTT was greater than that observed for ITT or clamps in vitro lets us suggest that *Ocy-PPARγ*$^{-/-}$ mice may have enhanced glucose-stimulated insulin secretion. Unfortunately, we were unable to test this directly, owing to insufficient blood samples; therefore, this should be tested in future studies in order to solve the discrepancies with the lesser insulin content seen in islets. Hence, deletion of PPARγ in bone improved glucose homeostasis by targeting mainly fat and liver metabolism without any major effect on muscle. The absence of a metabolic phenotype at 3 months of age emphasizes our previous finding of the important role of PPAR in the aging process with an exponential increase around the age of 4 months (32). When subjected to an HFD, *Ocy-PPARγ*$^{-/-}$ mice gained less weight than WT littermates, and the AUC of *Ocy-PPARγ*$^{-/-}$ challenged with an HFD was equivalent to that of WT mice on the CD (normal chow). In these

conditions, *Ocy-PPARγ*$^{-/-}$ mice exhibited less fragile bone, steatosis, white and adipose mass, and more muscle force and brown adipose activity compared with WT. In vitro experiments using cocultures of bone and other cells confirmed that the conditioned media from primary OB-OCY cultures of *Ocy-PPARγ*$^{-/-}$ mice have the capacity to decrease hepatocytic steatosis, increase insulin secretion by β-cells, and increase lipid oxidation by adipocytes. Hence, late OB-OCY secreted some osteokines regulated by PPARγ, which secondarily affected hepatocytes, β-cells, and adipocytes. Osteocalcin was the first osteokine able to control glucose homeostasis (10,11,33–35). However, both total and undercarboxylated osteocalcin were unchanged both in vivo and in vitro. In addition, compared with osteocalcin these osteokines seemed to not affect muscle metabolism. Sclerostin is able to control anabolic metabolism in adipocytes. More specifically, Sost$^{-/-}$ mice have a reduction in adipocyte size, with an improvement of glucose tolerance and enhancement of insulin sensitivity in WAT with concomitant increase of PPARgc1a and Ucp-1, i.e., markers of browning (36). From our gene expression analysis, BMP7 increase in *Ocy-PPARγ*$^{-/-}$ mice could also explain this metabolic phenotype. BMP7 is known to stimulate browning and reduce steatosis through an endocrine mechanism (37–40). Interestingly, BMP7 levels in the CM and serum of *Ocy-Pparγ*$^{-/-}$ were also higher compared with *Ocy-Pparγ*$^{+/+}$. Moreover, adding BMP7-neutralizing antibody in *Ocy-Pparγ*$^{-/-}$ CM did block its effects on FA oxidation in hepatocytes and adipocytes. Last, administration of a BMP7-neutralizing antibody in vivo blocked the hypoglycemia described in *Ocy-Pparγ*$^{-/-}$ mice. Considering the molecular weight of BMPs from 10 to 50 kDa, it is very plausible that osteocytes actively secrete BMP through the lacunacanalicular system, as we now know that small proteins (<70 kDa) circulate not only through the osteocyte lacunocanalicular network (41–43) but also secondarily to other tissues and act as a mediator of systemic metabolism (44).

There are several limitations to our study. Firstly, we used the Dmp1-cre promotor to delete PPARγ. Dmp1-Cre has previously been used as a specific promotor for late OB-OCY; however, more recently it has also been shown to be slightly expressed in skeletal muscle (45,46). Notwithstanding, *Ocy-PPARγ*$^{-/-}$ mice did not exhibit major skeletal muscle phenotype, as indicated by movement data, hyperinsulinemic-euglycemic clamp, and/or PET/CT analysis. Moreover, if deletion of PPARγ were dominant in skeletal muscle, which was not the case as indicated by Western blot and quantitative RT-PCR, we should have insulin resistance (47). On the contrary, we had an increase in insulin sensitivity, arguing definitively that the small deletion of PPARγ in muscle using the Dmp1-Cre system does not have a major effect in our model. Contrary to Lim et al. (48), we did not see any expression of Dmp1-Cre in the brain or intestine. Secondly, we were not able at this time point to elucidate all osteokines regulated by PPARγ that can explain the energy metabolism of our *Ocy-PPARγ*$^{-/-}$ mice. However, we know that it is not explained by changes in total or decarboxylated osteocalcin and that BMP7 is partially involved. Increased expression and/or activation of PPARγ in bone tissue has been involved in the pathophysiology of diabetes-induced bone fragility (32). Therefore, our new findings suggest that PPARγ in late OB-OCY not only contributes to regulate bone remodeling but also plays a critical function in glucose metabolism through both an increase of glucose uptake by the bone tissue itself and targeting key organs of energy metabolism, such as pancreas, adipose tissue, and liver, by secretion of osteokines other than osteocalcin, such as BMP7. Hence, this work brings new insights into the role that the skeletal tissue could play in pathophysiological processes leading to obesity, metabolic syndrome, and diabetes.

Acknowledgments. The authors thank Serge Ferrari (Geneva University Hospitals, Switzerland) for discussions and critical reading, Lynda Bonewald (University of Missouri–Kansas City) for providing the Dmp1-*cre*, and Beatrice Desvergne (University of Lausanne, Lausanne, Switzerland) for the *PPARγL2* mice. The authors thank Madeleine Lachize, Juliette Cicchini, and Pierre Apostolides for technical assistance with the bone tissue investigation (Service des Maladies Osseuses, University of Geneva, Switzerland). As a platform, the authors thank Christelle Veyrat-Durebex (Département de Physiologie Cellulaire et Métabolisme [PHYME], University of Geneva, Switzerland) for performing the hyperinsulinemic-euglycemic clamp, Jorge Altirriba Gutierrez (PHYME) for the LabMaster analysis, Clarissa Bartley (PHYME) for the β-cell extraction and coculture, and Didier Collin (Geneva University Hospitals, Switzerland) for the PET/CT analysis.

Funding. This work was supported by a grant from Novartis, formerly Ciba-Geigy-Jubilee-Foundation; the Bo & Kerstin Hjelt Foundation; and the Sir Jules Thorn Charitable Overseas Trust Reg. (to N.B).

Duality of Interest. No potential conflicts of interest relevant to this article were reported.

Author Contributions. N.B. conceived the study. M.T., P.M., M.F., and N.B. developed the methodology. J.B., F.B., and N.B. performed formal analysis and investigation. N.B. performed writing and original draft preparation. M.T., P.M., F.B., M.F., and N.B. reviewed and edited the manuscript. N.B. acquired funding. N.B., M.T., P.M., M.F., and N.B. provided resources. N.B. supervised the study. N.B. is the guarantor of this work and, as such, had full access to all the data in the study and takes responsibility for the integrity of the data and the accuracy of the data analysis.

References

1. Wan Y, Chong LW, Evans RM. PPAR-gamma regulates osteoclastogenesis in mice. Nat Med 2007;13:1496–1503

2. Kawai M, Sousa KM, MacDougald OA, Rosen CJ. The many facets of PPAR-gamma: novel insights for the skeleton. Am J Physiol Endocrinol Metab 2010;299: E3–E9

3. Cao J, Ou G, Yang N, et al. Impact of targeted PPARγ disruption on bone remodeling. Mol Cell Endocrinol 2015;410:27–34

4. Sun H, Kim JK, Mortensen R, Mutyaba LP, Hankenson KD, Krebsbach PH. Osteoblast-targeted suppression of PPARγ increases osteogenesis through activation of mTOR signaling. Stem Cells 2013;31:2183–2192

5. Fulzele K, Riddle RC, DiGirolamo DJ, et al. Insulin receptor signaling in osteoblasts regulates postnatal bone acquisition and body composition. Cell 2010;142: 309–319

6. Ferron M, McKee MD, Levine RL, Ducy P, Karsenty G. Intermittent injections of osteocalcin improve glucose metabolism and prevent type 2 diabetes in mice. Bone 2012;50:568–575

7. Wei J, Ferron M, Clarke CJ, et al. Bone-specific insulin resistance disrupts whole-body glucose homeostasis via decreased osteocalcin activation. J Clin Invest 2014;124:1–13
8. Brennan-Speranza TC, Henneicke H, Gasparini SJ, et al. Osteoblasts mediate the adverse effects of glucocorticoids on fuel metabolism. J Clin Invest 2012;122: 4172–4189
9. Levinger I, Lin X, Zhang X, et al. The effects of muscle contraction and recombinant osteocalcin on insulin sensitivity ex vivo. Osteoporos Int 2016;27:653–663
10. Yoshikawa Y, Kode A, Xu L, et al. Genetic evidence points to an osteocalcin-independent influence of osteoblasts on energy metabolism. J Bone Miner Res 2011; 26:2012–2025
11. Rodríguez-Carballo E, Gámez B, Méndez-Lucas A, et al. p38α function in osteoblasts influences adipose tissue homeostasis. FASEB J 2015;29:1414–1425
12. Mu Q, Fang X, Li X, et al. Ginsenoside Rb1 promotes browning through regulation of PPARγ in 3T3-L1 adipocytes. Biochem Biophys Res Commun 2015;466: 530–535
13. Jeremic N, Chaturvedi P, Tyagi SC. Browning of white fat: novel insight into factors, mechanisms, and therapeutics. J Cell Physiol 2017;232:61–68
14. Peyrou M, Bourgoin L, Poher AL, et al. Hepatic PTEN deficiency improves muscle insulin sensitivity and decreases adiposity in mice. J Hepatol 2015;62:421–429
15. Braga M, Reddy ST, Vergnes L, et al. Follistatin promotes adipocyte differentiation, browning, and energy metabolism. J Lipid Res 2014;55:375–384
16. Gamas L, Matafome P, Seiça R. Irisin and myonectin regulation in the insulin resistant muscle: implications to adipose tissue: muscle crosstalk. J Diabetes Res 2015;2015:359159
17. Wei J, Shimazu J, Makinistoglu MP, et al. Glucose uptake and Runx2 synergize to orchestrate osteoblast differentiation and bone formation. Cell 2015;161:1576–1591
18. Bozec A, Bakiri L, Jimenez M, et al. Osteoblast-specific expression of Fra-2/AP-1 controls adiponectin and osteocalcin expression and affects metabolism. J Cell Sci 2013;126:5432–5440
19. Izawa T, Rohatgi N, Fukunaga T, et al. ASXL2 regulates glucose, lipid, and dkeletal homeostasis. Cell Reports 2015;11:1625–1637
20. Aarden EM, Burger EH, Nijweide PJ. Function of osteocytes in bone. J Cell Biochem 1994;55:287–299
21. Javaheri B, Stern AR, Lara N, et al. Deletion of a single β-catenin allele in osteocytes abolishes the bone anabolic response to loading. J Bone Miner Res 2014; 29:705–715
22. Thouverey C, Caverzasio J. Suppression of p38α MAPK signaling in osteoblast lineage cells impairs bone anabolic action of parathyroid hormone. J Bone Miner Res 2016;31:985–993
23. Trajkovski M, Hausser J, Soutschek J, et al. MicroRNAs 103 and 107 regulate insulin sensitivity. Nature 2011;474:649–653
24. Mouche S, Mkaddem SB, Wang W, et al. Reduced expression of the NADPH oxidase NOX4 is a hallmark of adipocyte differentiation. Biochim Biophys Acta 2007; 1773:1015–1027
25. Mai G, Nguyen TH, Morel P, et al. Treatment of fulminant liver failure by transplantation of microencapsulated primary or immortalized xenogeneic hepatocytes. Xenotransplantation 2005;12:457–464
26. Carobbio S, Ishihara H, Fernandez-Pascual S, Bartley C, Martin-Del-Rio R, Maechler P. Insulin secretion profiles are modified by overexpression of glutamate dehydrogenase in pancreatic islets. Diabetologia 2004;47:266–276
27. Bonnet N, Conway SJ, Ferrari SL. Regulation of beta catenin signaling and parathyroid hormone anabolic effects in bone by the matricellular protein periostin. Proc Natl Acad Sci U S A 2012;109:15048–15053
28. Suárez-Zamorano N, Fabbiano S, Chevalier C, et al. Microbiota depletion promotes browning of white adipose tissue and reduces obesity. Nat Med 2015;21: 1497–1501
29. Marciano DP, Kuruvilla DS, Boregowda SV, et al. Pharmacological repression of PPARγ promotes osteogenesis. Nat Commun 2015;6:7443
30. Mieczkowska A, Baslé MF, Chappard D, Mabilleau G. Thiazolidinediones induce osteocyte apoptosis by a G protein-coupled receptor 40-dependent mechanism. J Biol Chem 2012;287:23517–23526
31. Winkler DG, Sutherland MK, Geoghegan JC, et al. Osteocyte control of bone formation via sclerostin, a novel BMP antagonist. EMBO J 2003;22:6267–6276
32. Fu H, Desvergne B, Ferrari S, Bonnet N. Impaired musculoskeletal response to age and exercise in PPARβ(-/-) diabetic mice. Endocrinology 2014;155:4686–4696
33. Lee NK, Sowa H, Hinoi E, et al. Endocrine regulation of energy metabolism by the skeleton. Cell 2007;130:456–469
34. Ferron M, Hinoi E, Karsenty G, Ducy P. Osteocalcin differentially regulates beta cell and adipocyte gene expression and affects the development of metabolic diseases in wild-type mice. Proc Natl Acad Sci U S A 2008;105:5266–5270
35. Wei J, Hanna T, Suda N, Karsenty G, Ducy P. Osteocalcin promotes β-cell proliferation during development and adulthood through Gprc6a. Diabetes 2014;63: 1021–1031
36. Frey J, Kim S, Li Z, et al. Sclerostin influences body composition by regulating catabolic and anabolic metabolism in adipocytes. J Bone Miner Res 2016; 31(Suppl. 1):1034
37. Tseng YH, Kokkotou E, Schulz TJ, et al. New role of bone morphogenetic protein 7 in brown adipogenesis and energy expenditure. Nature 2008;454:1000–1004
38. Sugimoto H, Yang C, LeBleu VS, et al. BMP-7 functions as a novel hormone to facilitate liver regeneration. FASEB J 2007;21:256–264
39. Kinoshita K, Iimuro Y, Otogawa K, et al. Adenovirus-mediated expression of BMP-7 suppresses the development of liver fibrosis in rats. Gut 2007;56:706–714
40. Boon MR, van den Berg SA, Wang Y, et al. BMP7 activates brown adipose tissue and reduces diet-induced obesity only at subthermoneutrality. PLoS One 2013; 8:e74083
41. Wang L, Ciani C, Doty SB, Fritton SP. Delineating bone's interstitial fluid pathway in vivo. Bone 2004;34:499–509
42. Wang L, Wang Y, Han Y, et al. In situ measurement of solute transport in the bone lacunar-canalicular system. Proc Natl Acad Sci U S A 2005;102:11911–11916
43. Price C, Zhou X, Li W, Wang L. Real-time measurement of solute transport within the lacunar-canalicular system of mechanically loaded bone: direct evidence for load-induced fluid flow. J Bone Miner Res 2011;26:277–285
44. Juffer P, Jaspers RT, Lips P, Bakker AD, Klein-Nulend J. Expression of muscle anabolic and metabolic factors in mechanically loaded MLO-Y4 osteocytes. Am J Physiol Endocrinol Metab 2012;302:E389–E395
45. Bellido T, Saini V, Pajevic PD. Effects of PTH on osteocyte function. Bone 2013; 54:250–257
46. Gorski JP, Huffman NT, Vallejo J, et al. Deletion of Mbtps1 (Pcsk8, S1p, Ski-1) gene in osteocytes stimulates soleus muscle regeneration and increased size and contractile force with age. J Biol Chem 2016;291:4308–4322
47. Hevener AL, He W, Barak Y, et al. Muscle-specific Pparg deletion causes insulin resistance. Nat Med 2003;9:1491–1497
48. Lim J, Burclaff J, He G, Mills JC, Long F. Unintended targeting of Dmp1-Cre reveals a critical role for Bmpr1a signaling in the gastrointestinal mesenchyme of adult mice. Bone Res 2017;5:16049